

Highlights

Data-efficient flood depth prediction through domain-aware coresets selection and tabular foundation models

Lipai Huang, Adithi Srinath, Manas Singh, Junwei Ma, Ali Mostafavi

- A two-stage coreset jointly stratifies by storm return period and spatial structure.
- A vanilla foundation model matches the watershed-level baseline with a 50k coreset.
- In-context learning predicts a held-out watershed from neighbors without retraining.
- Models extrapolate on out-of-distribution storms and remain accurate in-distribution.

Data-efficient flood depth prediction through domain-aware coresets selection and tabular foundation models

Lipai Huang^{a,*}, Adithi Srinath^b, Manas Singh^b, Junwei Ma^{a,c} and Ali Mostafavi^{a,d}

^aUrban Resilience.AI Lab, Zachry Department of Civil and Environmental Engineering, Texas A&M University, College Station, TX, USA

^bDepartment of Computer Science and Engineering, Texas A&M University, College Station, TX, USA

^cResilitix Intelligence LLC, Houston, TX, USA

^dInstitute for a Disaster Resilient Texas, Texas A&M University, College Station, TX, USA

ARTICLE INFO

Keywords:

Domain-aware coresets construction
In-context learning
Tabular foundation model
Flood depth prediction
Cross-watershed transferability
Hydrodynamic surrogate

ABSTRACT

Near-real-time flood depth prediction demands surrogate models that are accurate, fast, and transferable across watersheds. Supervised surrogates can match physics-based simulators in accuracy but need millions of training rows per watershed and cannot extrapolate beyond their original mesh. We propose a domain-aware coresets construction pipeline that conditions a tabular foundation model at inference time. The pipeline stratifies storms by return period and most-affected watershed, then samples hexagons with a target-aware spatial selector. With 0.7% of the per-watershed training pool, the model attains a mean R^2 of 0.663 across nine Houston-area watersheds, within 98.5% of the supervised reference ($R^2 = 0.673$). It transfers to held-out watersheds without task-specific retraining, staying ahead of a coresets-trained supervised baseline. On real storms it exceeds the supervised reference on a far out-of-distribution case and trails it on a mostly in-distribution one. Domain-aware coresets construction lets tabular foundation models deliver data-efficient, watershed-transferable flood predictions without per-watershed training.

1. Introduction

Timely flood depth information supports emergency managers and infrastructure operators during extreme weather events, and also underpins downstream assessments of flood exposure (Yin and Mostafavi, 2023), mobility disruption, and community resilience (Yin, Li and Mostafavi, 2026). Yet generating it at scale remains computationally demanding (Li, Ma, Brody and Mostafavi, 2025). Physics-based hydrodynamic models such as the Hydrologic Engineering Center’s River Analysis System (HEC-RAS) provide the engineering reference for inundation depth prediction. Their cost grows quickly with simulated extent and mesh resolution, especially when many storm events must be screened. A direct HEC-RAS sweep is therefore impractical for near-real-time forecasting or broad scenario testing (Ma, Li, Li and Mostafavi, 2026). Machine learning (ML) surrogates trained on simulator output have become a standard alternative and offer near-instant inference once trained (Bentivoglio, Isufi, Jonkman and Taormina, 2022; Mosavi, Ozturk and Chau, 2018).

Existing surrogate work falls into two patterns. The first trains one model per mesh cell, capturing local dynamics at fine resolution while producing a fragmented collection that cannot be applied beyond the original mesh (Lee, Huang, Antolini, Garcia, Juan, Brody and Mostafavi, 2024). The second trains a single supervised model on the full knowledge base of one watershed, which yields strong in-watershed accuracy but binds the predictor to its training region (Zahura, Goodall, Sadler, Shen, Morsy and Behl, 2020). Both patterns share the same operational drawback:

each requires millions of training rows, and adding a new watershed or recalibrating after an event-regime shift entails another full training pass. Tree-based gradient boosting (Chen and Guestrin, 2016) still dominates this space because deep tabular methods continue to underperform tree ensembles on structured input (Grinsztajn, Oyallon and Varoquaux, 2022). Deep learning has produced striking results on adjacent hydrologic tasks such as rainfall-runoff modeling (Kratzert, Klotz, Brenner, Schulz and Herrnegger, 2018), but for spatially distributed flood-depth surrogates the tree-based pattern remains the practical default.

Transformer and foundation-model architectures have recently been adapted to structured disaster-management tasks, including post-disaster building-damage categorization (Xiao and Mostafavi, 2025), multimodal impact assessment (Xiao, Yin and Mostafavi, 2026), and graph-based damage prediction (Esparza, Battala and Mostafavi, 2026). Tabular foundation models (TFMs) such as TabPFN (Hollmann, Müller, Purucker, Krishnakumar, Körfer, Hoo, Schirrmeyer and Hutter, 2025) and TabICL (Qu, Holzmüller, Varoquaux and Le Morvan, 2024) offer a different path. A TFM is a single transformer pretrained on a wide distribution of synthetic tabular tasks. It solves a new task at inference time by conditioning on a labeled context set rather than through gradient updates. This in-context learning (ICL) framing avoids per-task retraining, and a sufficiently strong pretrained backbone can rival task-specific supervised models on tabular benchmarks. However, the context windows of the tabular foundation models considered in this work are bounded at roughly 10^4 to 10^5 rows (Hollmann et al., 2025; Grinsztajn, Flöge, Key, Birkel, Jund, Roof, Jäger, Hollmann and Hutter, 2025; Qu et al., 2024), while a single watershed’s simulation knowledge base typically reaches millions.

*Corresponding author

✉ lipai.huang@tamu.edu (L. Huang)

ORCID(s): 0009-0005-3732-7319 (L. Huang)

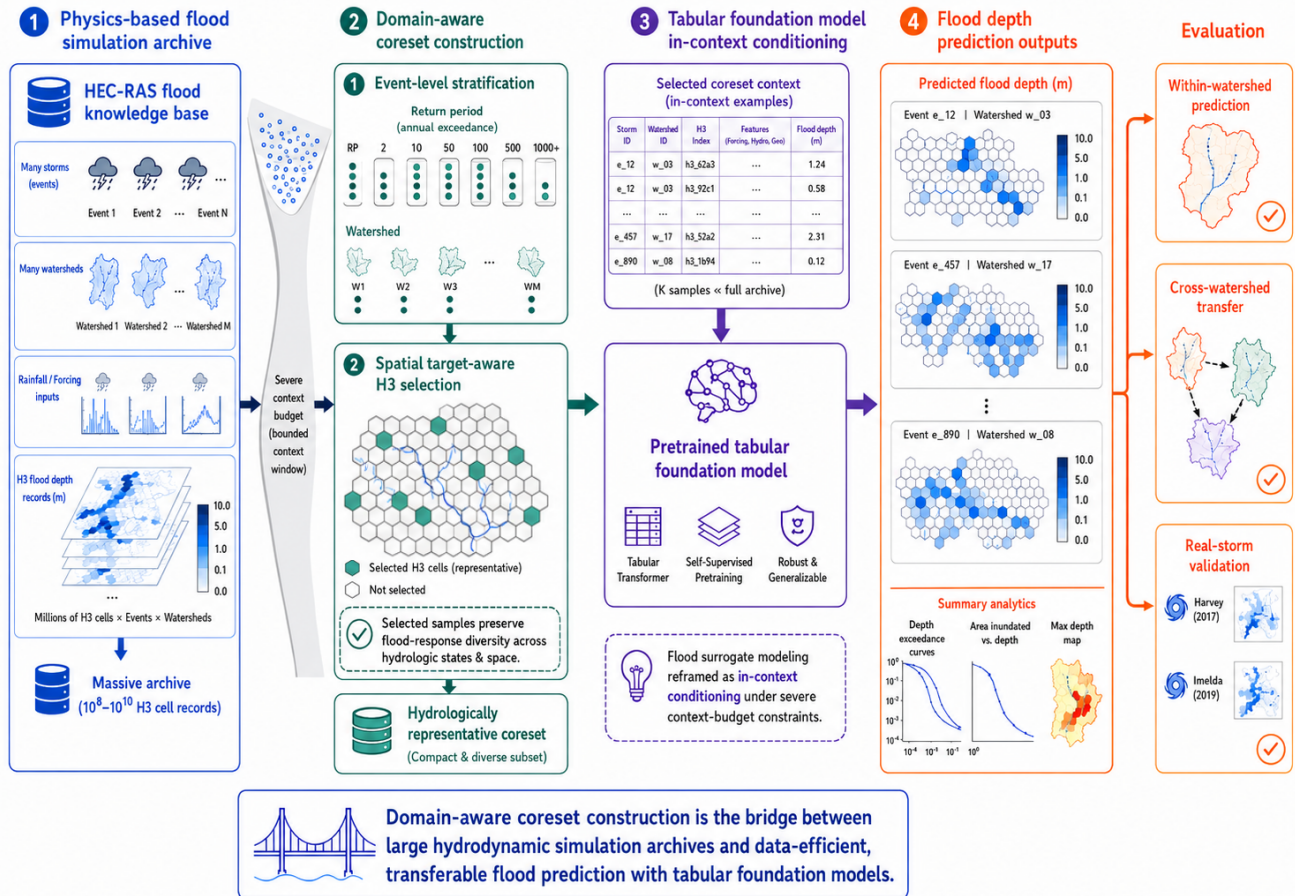


Figure 1: Conceptual overview of the proposed approach. (1) Physics-based flood simulation archive: a HEC-RAS knowledge base of 592 synthetic storm events across nine Houston-area watersheds, on the order of 10^8 event-hexagon rows, with storm metadata, watershed boundaries, and NOAA Atlas 14 return-period labels. (2) Domain-aware coreset construction: a two-stage pipeline compresses the archive into a compact, hydrologically representative subset. Stage 1 stratifies events by return period and most-affected watershed, and Stage 2 selects H3 Level 10 hexagons with a target-aware facility-location strategy. (3) Tabular foundation model in-context conditioning: the coreset conditions a pretrained tabular foundation model at inference, with no per-watershed fine-tuning. (4) Flood-depth prediction outputs: the model returns peak inundation depth for query hexagons. The pipeline is evaluated under three protocols: within-watershed accuracy, cross-watershed leave-one-out transfer, and real-storm validation on Hurricane Harvey and Tropical Storm Imelda. (The schematic was prepared with the assistance of ChatGPT-5.5.)

Choosing which rows to put into the context becomes the central operational question. Naive options such as random sampling or feature-only facility location ignore the spatial autocorrelation and event-magnitude imbalance that govern flood data. Building a high-quality coreset for a TFM in this setting therefore depends on encoding hydrologic and geographic prior knowledge into the selection step.

Figure 1 summarizes the proposed approach. We propose that a TFM conditioned on a carefully built coreset is a feasible flood-depth surrogate at the watershed level. We then test how far the same configuration transfers to held-out watersheds under a leak-free protocol. To support both questions we develop a domain-aware coreset construction pipeline that operates in two stages. Stage one stratifies storm events on two axes: storm return period (RP) and most-affected watershed. The dual stratification ensures that rare high-RP events and their host watersheds survive sampling

noise. Stage two samples from a hierarchical hexagonal (H3) grid at Level 10 with cell edge length of approximately 75 m. The selector combines facility-location coverage in static-feature space with a z-scored target-depth signal. For cross-watershed evaluation we adopt a leave-one-out (LOO) protocol in which the held-out target watershed contributes neither training rows nor context.

The contributions of this paper are:

- A two-stage domain-aware coreset construction pipeline that combines event-level stratification by return period and watershed with target-aware hexagon selection, encoding hydrologic and geographic priors in the context.
- A demonstration that a vanilla TFM conditioned on the domain-aware coreset (about 0.7% of the per-watershed training pool) recovers 98.5% of a

watershed-level supervised reference in average R^2 across nine Houston-area watersheds.

- A leak-free leave-one-out protocol with two source-selection modes (neighboring versus all other watersheds), showing that the same vanilla TFM transfers to held-out watersheds without retraining and outperforms a coreset-trained supervised baseline at most context sizes in both modes.

2. Related Work

2.1. Return Period for Storm Stratification

Hydrology distinguishes pluvial return period (RP) from fluvial RP by their driver. Pluvial RP ranks events by short-duration rainfall intensity and supports urban drainage design where local rainfall dominates. Fluvial RP ranks events by streamflow magnitude at a gauge and supports riverine flood mapping where upstream runoff dominates. The two can rank the same storm differently, so combined RP frameworks treat both drivers jointly and are preferred in mixed-regime basins where rainfall and runoff co-vary (Zscheischler, Westra, van den Hurk, Seneviratne, Ward, Pitman, AghaKouchak, Bresch, Leonard, Wahl and Zhang, 2018; Wahl, Jain, Bender, Meyers and Luther, 2015). All variants share the same statistical foundation: a T -year storm has a $1/T$ chance of being equaled or exceeded in any single year. RP underpins floodplain mapping, hydraulic structure design, and insurance rate setting. In the United States the reference curves are published in NOAA Atlas 14 (National Oceanic and Atmospheric Administration, 2018), which maps storm duration and accumulated rainfall depth to RP at the county level. For supervised flood-prediction datasets, synthetic storm libraries tend to oversample moderate events, so intentional stratification by RP is needed to keep rare, high-impact storms from being under-represented in training (Bentivoglio et al., 2022).

2.2. Coreset Selection

A coreset is a small, weighted subset of a dataset chosen so that a model trained or conditioned on the subset behaves similarly to one trained on the full data (Phillips, 2017; Mirzasoleiman, Bilmes and Leskovec, 2020; Bachem, Lucic and Krause, 2017). Coreset selection methods fall into three broad families. Uniform random sampling provides an unbiased default but covers feature space inefficiently when data are imbalanced. Geometric methods such as facility location (Lin and Bilmes, 2011; Wei, Iyer and Bilmes, 2015) and core-set covering (Sener and Savarese, 2018) greedily pick samples that maximize coverage of a feature-space kernel, offering diversity guarantees but ignoring labels. Target-aware methods incorporate label statistics: gradient-based selectors (Killamsetty, Sivasubramanian, Ramakrishnan and Iyer, 2021b; Killamsetty, Sivasubramanian, Ramakrishnan, De and Iyer, 2021a) pick samples whose gradients best approximate the full-batch update, proxy-based selectors (Coleman, Yeh, Musmann, Mirzasoleiman, Bailis, Liang, Leskovec and Zaharia, 2020) rank candidates with a cheaper

surrogate model, and pruning metrics such as forgetting score or supervised classification margin separate redundant from informative examples (Sorscher, Geirhos, Shekhar, Ganguli and Morcos, 2022). In the foundation-model era, coreset selection has taken on a second role of choosing in-context examples that condition a pretrained predictor at inference time (Hollmann et al., 2025; Thomas, Ma, Hosseinzadeh, Golestan, Yu, Volkovs and Caterini, 2024). Most of these methods assume samples are independent, an assumption that breaks in geophysical applications where features are strongly autocorrelated, causing naive feature-space selection to cluster samples geographically and leave parts of the domain unrepresented (Roberts, Bahn, Ciuti, Boyce, Elith, Guillera-Arroita, Hauenstein, Lahoz-Monfort, Schröder, Thuiller, Warton, Wintle, Hartig and Dormann, 2017; Meyer, Reudenbach, Hengl, Katurji and Nauss, 2018).

2.3. In-Context Learning for Tabular Prediction

Tabular foundation models (TFMs) cast tabular prediction as in-context learning: a transformer is pretrained once on a large distribution of synthetic tasks and, at inference, conditions on a labeled context set $(\mathbf{X}_{ctx}, \mathbf{y}_{ctx})$ to predict labels for a query set \mathbf{X}_q without gradient updates. The framing originates in the prior-data fitted networks of Müller, Hollmann, Pineda Arango, Grabocka and Hutter (2022) and was specialized to tabular classification and regression by TabPFN (Hollmann, Müller, Eggenesperger and Hutter, 2023; Hollmann et al., 2025). Subsequent releases progressively expand the supported context: TabPFN-v2.5 (Grinsztajn et al., 2025) reaches roughly 5×10^4 rows, and TabPFN-v2.6 (Prior Labs, 2025) extends this to 10^5 rows. TabICL (Qu et al., 2024) targets even larger context sizes through a column-then-row attention mechanism. A separate strand augments these backbones with task-specific fine-tuning (Thomas et al., 2024), with full fine-tuning recently shown to be a stable baseline for TabPFN-v2 (Rubachev, Kotelnikov, Kartashev and Babenko, 2025). Transfer learning has likewise been used to improve tabular prediction from limited engineering data (Pak, Leach, Yoon and Paal, 2023).

2.4. Out-of-Distribution Evaluation

Spatially distributed predictors are vulnerable to two distinct evaluation failures. Standard random k -fold cross-validation underestimates prediction error on spatially autocorrelated data, because train and test folds remain close in feature and physical space (Roberts et al., 2017). Spatial cross-validation schemes such as Leave-Location-Out hold out entire spatial blocks to break that contamination (Meyer et al., 2018). A separate question is whether predictions made outside the training distribution can be trusted at all: Meyer and Pebesma (2021) formalize this as the Area of Applicability of a spatial model, and the WILDS benchmark (Koh, Sagawa, Marklund, Xie, Zhang, Balsubramani, Hu, Yasunaga, Phillips, Gao et al., 2021) catalogues representative distribution shifts in machine learning.

3. Data

The primary data is the MaxFloodCast HEC-RAS simulation database (Lee et al., 2024) covering nine watersheds in Harris County, Texas (Figure 2). Harris County is the largest county in the Greater Houston Metropolitan Statistical Area, with a substantially flat topography ranging from roughly -12 m to 91 m above mean sea level and a population exceeding 4.5 million. Two main hydrologic systems organize the county: Cypress Creek in the north and the Buffalo Bayou system across the central and southern portions, both draining eastward through the San Jacinto River and the Ship Channel into the Gulf of Mexico.

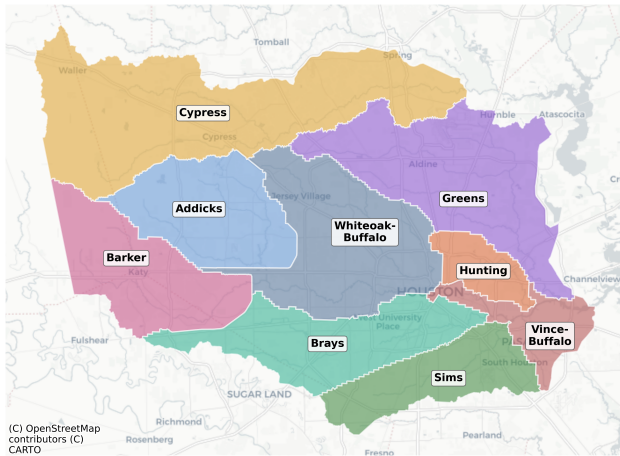


Figure 2: The nine Houston-area watersheds, dissolved from the HEC-RAS simulation mesh. Basemap rendered with contextily (<https://contextily.readthedocs.io/en/latest/index.html>) using OpenStreetMap and CARTO tiles.

The database contains 592 synthetic storm events generated by applying a Rasterized Time-series Resampling Method to historic storms in the area, with durations from 1 to 33 hours and hourly rainfall grids at approximately 1,010 m resolution. Flood inundation depths are simulated by HEC-RAS 2D over an unstructured mesh of 26,301 cells (nominal size ≈ 366 m), refined along major watercourses and breaklined at high-elevation features. From this database we inherit the cell-level peak inundation depth target and the per-event rainfall metadata. All other inputs are processed independently in this study.

To establish a uniform spatial unit across all variables, we discretize each mesh cell into H3 Level 10 hexagons (about 75 m edge length) via polygon polyfill (≈ 7.7 hexagons per mesh cell on average). Static geophysical features are extracted from external geospatial datasets and resampled onto the resulting 177,330 hexagons. The HEC-RAS depth output and event-level rainfall metadata are likewise resampled to the same H3 Level 10 grid. Hexagons in the same mesh cell share that cell's dynamic features (rainfall, depth) but carry their own static features, yielding $592 \text{ events} \times 177,330 \text{ hexagons} \approx 105$ million rows with no missing values. Per-watershed counts range from 2.2 M

(Hunting Bayou) to 14.1 M (Cypress Creek), with a mean of about 6.9 M.

Each row carries 11 predictors and a target (Table 1). Eight static predictors describe local topography and hydrology: elevation, imperviousness, Topographic Wetness Index (TWI), road density within a 500 m radius, distance to coast, Height above Nearest Drainage (HAND), distance to the nearest stream, and distance to the nearest stream of order ≥ 4 . Three dynamic predictors describe each storm: cumulative rainfall, peak rainfall intensity, and precipitation duration. Among the static predictors, TWI follows the standard $\ln(\text{SCA} / \tan \beta)$ formulation under D_∞ flow routing (Tarboton, 1997) computed in SAGA GIS (Conrad, Bechtel, Bock, Dietrich, Fischer, Gerlitz, Wehberg, Wichmann and Böhner, 2015), and road density is the fraction of road area within a 500 m circular kernel applied to a 15 m-buffered roadway raster. The target is the per-event peak inundation depth at each hexagon simulated by HEC-RAS. The model predicts one peak-depth value per event and hexagon from static geospatial features and aggregated rainfall descriptors, not a time-evolving nowcast that updates depth as new rainfall or gauge data arrive.

Each storm is annotated with two derived fields used for stratification. The most-affected watershed is the watershed whose cells have the highest mean inundation depth during that storm. The RP bin assigns each storm to the largest exceeded NOAA Atlas 14 (National Oceanic and Atmospheric Administration, 2018) county-median threshold at the PFDS duration class matching the event's storm duration, with the procedure detailed in Section 4.1. RP is used as a stratification label rather than a model input. Bin populations cover the range from below 1-year through 1,000-year, with 42 events each in the 500-year and 1,000-year bins.

The 592 events are split into 350 for training, 121 for validation, and 121 for testing under double stratification on RP bin and most-affected watershed, with a post-processing pass that prevents any single watershed from being under-represented at test time. Within the test set, 42 stratified-subsample events serve as the query set in all experiments.

For external validation we use two real storms simulated with observed rainfall: Hurricane Harvey (August 2017) and Tropical Storm Imelda (September 2019). Rainfall inputs come from Harris County Flood Control District rain-gage observations (Harris County Flood Control District, 2023) interpolated through Thiessen polygons, while depth targets are produced by HEC-RAS 2D under the same setup as the synthetic events and resampled onto the same H3 L10 grid. Harvey lies entirely outside the synthetic training envelope on the (cumulative rainfall, duration) plane and is treated as fully out-of-distribution (OOD). Imelda mixes in-distribution and OOD cells.

4. Methodology

4.1. Return Period Construction

Each storm event is labeled with a single RP bin used to stratify the dataset split and the Stage 1 event selection. The

Table 1

Key variables used in modeling and event stratification, with data sources.

Category	Variable	Data Source
Topography	Elevation	National Elevation Dataset (NED)
	Imperviousness	National Land Cover Database (NLCD)
	Topographic Wetness Index (TWI)	NED + NLCD
	Road Density within 500 m radius	TxDOT roadway network
	Distance to Coast	National Hydrography Dataset Plus High Resolution (NHDPlusHR)
Hydrology	Height above Nearest Drainage (HAND)	NOAA National Water Model
	Distance to Nearest Stream	NHDPlusHR
	Distance to Stream (order ≥ 4)	NHDPlusHR
Aggregated Event-specific	Cumulative Rainfall	HEC-RAS 2D
	Peak Rainfall Intensity	HEC-RAS 2D
	Precipitation Duration	HEC-RAS 2D
Event Annotation	Return Period (RP)	NOAA Atlas 14

event is first assigned a NOAA Atlas 14 duration class d^* based on its storm duration d_e :

$$d^* = \begin{cases} 6 \text{ h}, & d_e \leq 6 \text{ h} \\ 12 \text{ h}, & 6 \text{ h} < d_e \leq 12 \text{ h} \\ 24 \text{ h}, & d_e > 12 \text{ h} \end{cases} \quad (1)$$

which selects the smallest NOAA Atlas 14 (National Oceanic and Atmospheric Administration, 2018) class containing d_e . The event's peak cumulative rainfall across hexagons, r_{\max} , is then compared against the Harris-County-median NOAA Atlas 14 thresholds $\{\tau_{d^*,T}\}$ at the candidate return periods $T \in \{1, 2, 5, 10, 25, 50, 100, 200, 500, 1000\}$ years, and the event is assigned the largest T for which the threshold is exceeded:

$$\text{RP}_{\text{event}} = \max\{T : r_{\max} \geq \tau_{d^*,T}\}, \quad (2)$$

with $\text{RP}_{\text{event}} = 0$ when no threshold is exceeded.

4.2. Two-Stage Coreset Construction

The choice of in-context examples is the central design decision of this paper. A naive random sample of the simulation knowledge base ignores two properties of flood data: storm-magnitude imbalance leaves rare high-RP events sparse in any such subsample, and spatial autocorrelation among static features causes the picked hexagons to cluster geographically. We address both with a two-stage construction: events are first dual-stratified by return period and watershed, then hexagons within each watershed are sampled with a target-aware spatial selector. The resulting coreset is the Cartesian product of N_e events sampled in Stage 1 and N_h hexagons selected per watershed in Stage 2, giving $N = N_e \times N_h$ rows per watershed. Table 2 lists the (N_e, N_h) values used for each N .

The decomposition balances event diversity against per-watershed hexagon coverage within a context that fits all TFMs evaluated. The largest size $N = 50\text{k}$ matches TabPFN-v2.5's native context limit, so every coreset-based

Table 2

 Coreset decomposition: (N_e, N_h) for each per-watershed size N .

N	N_e	N_h
500	20	25
1,000	25	40
2,000	40	50
5,000	50	100
10,000	50	200
50,000	50	1,000

model sees the same maximum context regardless of its own capacity ceiling. Within this N envelope, both N_e and N_h rise at small N so the coreset captures both event types and watershed geometry. N_e saturates at 50 once N allows it, which keeps Stage 1 from depleting the rare-RP tail bins where the training pool itself is sparse. N_h then grows to keep $N = N_e \times N_h$ as N continues to climb.

4.2.1. Stage 1: Event Stratification

Given N_e events to select in Stage 1, we draw them from the training split, stratified jointly by RP bin and most-affected watershed. Each watershed first gets a floor of $k_{\min} = \min(2, \lfloor N_e/n_{\text{ws}} \rfloor)$ events, where n_{ws} is the number of watersheds. The remaining slots are allocated across watersheds in proportion to their training-event counts (largest-remainder rounding), and within each watershed across its RP bins. By construction, every watershed contributes at least k_{\min} events, with within-watershed RP stratification preserving the pool's bin diversity.

4.2.2. Stage 2: Hexagon Selection

Within each watershed we evaluate five hexagon-selection methods: a Random baseline, Facility Location (FL), Spatial-Penalty FL (SP-FL), Depth-Stratified Sampling (Strat-Depth), and Depth-Augmented FL (FL-Depth).

Random. Uniform random sampling, used as a baseline.

FL. Greedy facility location on a feature-space RBF kernel (Lin and Bilmes, 2011; Wei et al., 2015; Sener and Savarese, 2018), evaluated over a candidate pool $\mathcal{H}_{\text{pool}}$ of 3,000 random hexagons subsampled from the watershed for tractability:

$$\mathcal{H}_{\text{fl}} = \arg \max_{|\mathcal{H}|=N_h} \sum_{h \in \mathcal{H}_{\text{pool}}} \max_{s \in \mathcal{H}} K(x_h, x_s), \quad (3)$$

$$K(x_h, x_s) = \exp\left(-\frac{\|x_h - x_s\|^2}{\sigma_f^2}\right), \quad (4)$$

where x_h is the z-scored static-feature vector of hexagon h and σ_f^2 is set by the median heuristic on pairwise squared distances within the pool.

SP-FL. Facility location on the same pool with a hard spatial-exclusion constraint:

$$\|p_{h_i} - p_{h_j}\|_{\text{geo}} \geq r_{\min}, \quad \forall h_i, h_j \in \mathcal{H}_{\text{sp-fl}}, i \neq j, \quad (5)$$

where p_h is the hexagon centroid and $\|\cdot\|_{\text{geo}}$ is haversine distance. We fix $r_{\min} = 300$ m. SP-FL can fall short of N_h in small watersheds when the geometric constraint exhausts available hexagons (Hunting Bayou 56% filled at $N = 50\text{k}$, Vince-Buffalo 71%).

Strat-Depth. Stratified random sampling on a per-hexagon depth signal y_h . The depth signal is the mean simulated peak depth at hexagon h over the Stage 1 event set \mathcal{E} for the current N :

$$y_h = \frac{1}{|\mathcal{E}|} \sum_{e \in \mathcal{E}} \text{depth}_{h,e}, \quad (6)$$

where $\text{depth}_{h,e}$ is the HEC-RAS-simulated peak depth at hexagon h in event e . Dry hexagons ($y_h \leq 0$) form a separate bin when present and wet hexagons are split into up to three quantile bins, for a total of at most four bins. Selections are allocated equally per bin with largest-remainder allocation to the largest pools for the residual.

FL-Depth. Facility location on the same pool with feature vector augmented by the z-scored depth signal from Eq. 6:

$$\tilde{x}_h = [x_h; z(y_h)], \quad z(y) = \frac{y - \mu_y}{\sigma_y}, \quad (7)$$

where μ_y and σ_y are the pool-wide mean and standard deviation of y_h . The kernel bandwidth σ_f^2 is recomputed by the median heuristic on the augmented \tilde{x} pool.

4.3. Models

4.3.1. Reference Baselines

Coreset-XGB is XGBoost (Chen and Guestrin, 2016) trained on a single coreset of $N = 50\text{k}$ rows per watershed, with hyperparameters from Lee et al. (2024): 1,000 histogram-based trees of maximum depth 5, learning rate 0.01, column subsampling rate 0.3, and L_1 regularization weight 10. Full-KB-XGB uses the same hyperparameters

but is trained on *all* 350 training events for that watershed, on average ≈ 6.9 M rows. We call it the supervised reference rather than a strict ceiling, since several coreset-based models exceed it on individual watersheds and on the far out-of-distribution storm.

4.3.2. Vanilla TFMs

We evaluate three vanilla TFMs. TabPFN-v2.6 (Hollmann et al., 2025; Prior Labs, 2025) is the latest release in the TabPFN family. TabPFN-v2.5 (Grinsztajn et al., 2025) provides a backbone version contrast, and TabICL (Qu et al., 2024) extends the comparison to a second TFM family. At inference time the coreset \mathcal{C} provides the in-context examples:

$$\hat{y}_q = f_\theta(x_q; \{(x_i, y_i)\}_{i \in \mathcal{C}}) \quad (8)$$

where f_θ is the pretrained transformer and θ is held fixed. No gradient updates are applied at inference.

4.3.3. Fine-Tuning Variants

To test whether fine-tuning (FT) improves over vanilla inference, we add two FT modes on both the TabPFN-v2.5 and TabPFN-v2.6 backbones. TabPFN-FT-v2.5 / v2.6 applies per-watershed fine-tuning on each watershed's own FL-Depth coreset. TabPFN-FTLOO-v2.5 / v2.6 is fine-tuned across the other eight watersheds, with each episode drawing context and query from one of those eight sampled uniformly at random, so that on a held-out target both context and weights are target-free. Both modes share a single recipe: 500 episodes with fresh context and query batches of 4,000 and 2,048 rows, AdamW at learning rate 10^{-5} and weight decay 10^{-4} , gradient clipping at 1.0, bfloat16 autocast, and MSE loss on context-normalized targets.

5. Experiments and Results

5.1. Coreset Construction

The coresets evaluated below come from the two-stage pipeline of Section 4.2, with event selection in Stage 1 and hexagon selection in Stage 2.

Stage 1 selects $N_e = 50$ training events. This is large enough for proportional allocation to give every watershed several events despite the uneven per-watershed training pools, and small enough for $N = N_e \times N_h$ to fit within TabPFN-v2.5's context cap. The allocation in Figure 3 combines proportional sampling with a floor of $k_{\min} = 2$, routing most of the sample to the larger bayou watersheds. The floor catches Addicks and Barker, whose small training pools would otherwise round to zero and exclude these watersheds from the downstream protocols. The below-1-year stratum visible at Addicks and Barker is a direct consequence of this floor on small pools. Each pool spans only 2 and 4 RP bins respectively, including a below-1-year bin, so the floor forces both watersheds to draw bins they would otherwise miss. The 500-year and 1,000-year classes each surface in four watersheds, providing rare-event coverage across the bayou network.

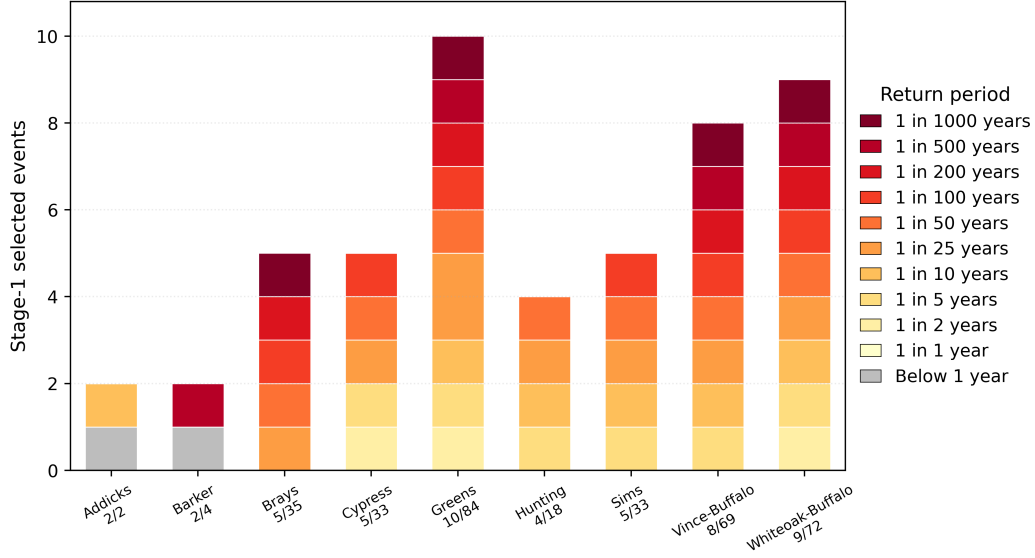


Figure 3: Per-watershed event allocation at $N_e = 50$. Bars stacked by return period bin, with x-axis labels showing the selected / training-pool ratio per watershed.

Table 3

Mean R^2 across nine watersheds for the five hexagon selectors at each coreset size N . Bold marks each column's best selector. FL-Depth has the highest cross- N average for both models, and XGB shows a smaller method spread than v2.5 at every N .

(a) Vanilla TabPFN-v2.5

Method	$N = 500$	$N = 1k$	$N = 2k$	$N = 5k$	$N = 10k$	$N = 50k$	Mean
Random	0.348	0.370	0.381	0.429	0.463	0.609	0.433
FL	0.315	0.283	0.277	0.346	0.393	0.609	0.371
SP-FL	0.320	0.307	0.298	0.377	0.417	0.602	0.387
Strat-Depth	0.381	0.442	0.453	0.409	0.471	0.611	0.461
FL-Depth	0.455	0.475	0.469	0.402	0.418	0.621	0.473

(b) Coreset-XGB

Method	$N = 500$	$N = 1k$	$N = 2k$	$N = 5k$	$N = 10k$	$N = 50k$	Mean
Random	0.400	0.427	0.425	0.486	0.524	0.601	0.477
FL	0.367	0.376	0.384	0.474	0.515	0.609	0.454
SP-FL	0.373	0.387	0.396	0.479	0.523	0.605	0.461
Strat-Depth	0.414	0.433	0.455	0.487	0.528	0.605	0.487
FL-Depth	0.436	0.466	0.469	0.458	0.514	0.606	0.491

Stage 2 selects N_h hexagons per watershed under five candidate selectors defined in Section 4.2.2. The selectors trade off feature-space coverage against spatial spread, illustrated for Brays Bayou at $N = 10k$ ($N_h = 200$) in Figure 4. FL clusters tightest because its feature-space objective does not penalize spatial proximity, so two nearby hexagons with distinct features can both be selected. Random and Strat-Depth lack any spatial term and follow the underlying mesh density. FL-Depth is more spread than these spatially neutral baselines because its feature vector includes the z-scored depth signal, which varies smoothly in space and therefore makes nearby hexagons redundant under the FL objective.

SP-FL has the widest spread under the $r_{\min} = 300$ m exclusion constraint.

To pick the downstream hexagon selector, we sweep Vanilla TabPFN-v2.5 as the representative TFM and Coreset-XGB as a tree-based control over all five methods at six N values, reported in Table 3. For v2.5 in panel (a), FL-Depth wins at four of the six N values and tops the cross- N average at $R^2 = 0.473$, with Strat-Depth second and the pure facility-location methods FL and SP-FL well behind. FL-Depth slips below Random at $N = 5k$ and below Strat-Depth at $N = 10k$, but these dips reflect the v2.5 backbone's weakness in this N range rather than any selector failure. Outside that mid- N window, depth-aware selectors dominate because

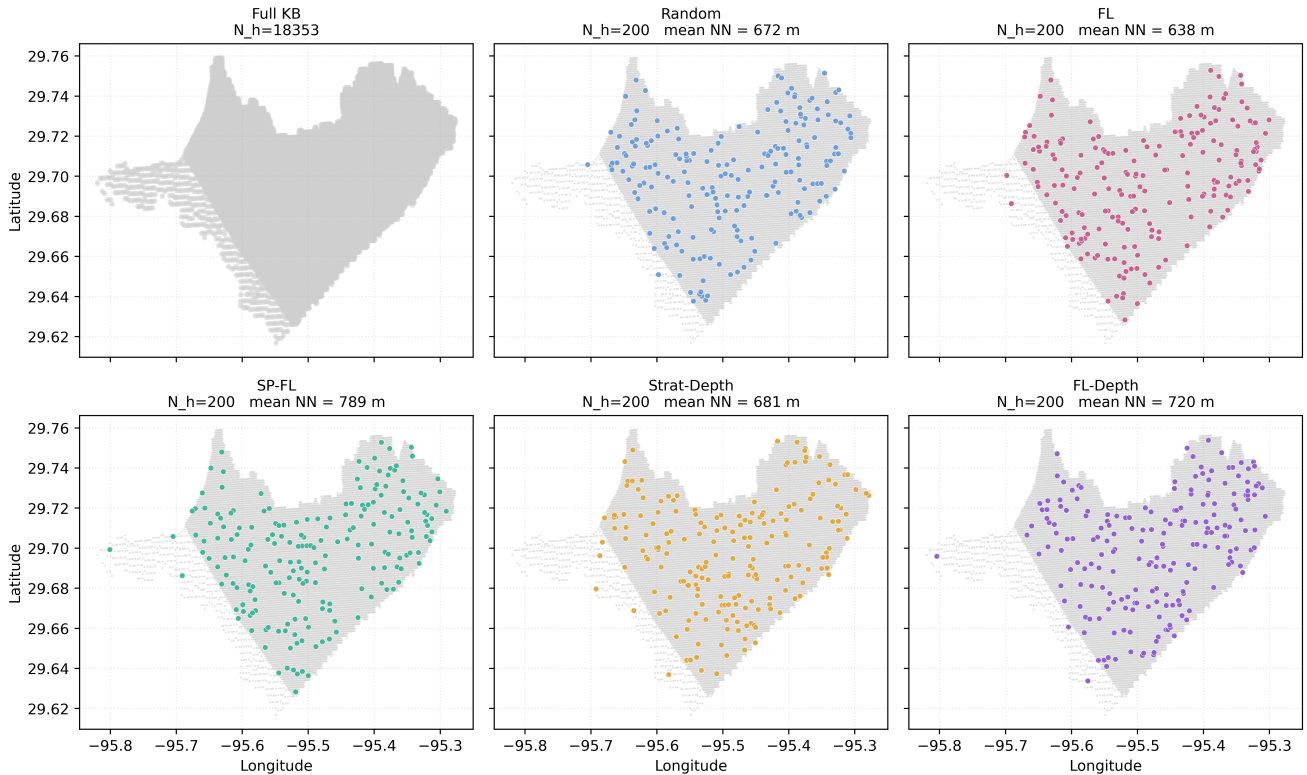


Figure 4: Spatial distribution of selected hexagons for Brays Bayou at $N = 10k$ ($N_h = 200$) under all five Stage 2 methods. Panel titles include the mean nearest-neighbor distance. The sparser sampling at the watershed’s southwestern arm reflects the underlying mesh, which thins out where the watershed narrows.

the per-hexagon depth signal compresses each hexagon’s response across the Stage 1 event mix into a single target-relevant dimension. The Stage 1 events span below-1-year through 1,000-year storms, so hexagons selected along this signal cover the flood-response surface directly. Pure feature-space selection picks hexagons that look feature-diverse but can still cluster on flood response, leaving the target distribution under-covered. The largest size $N = 50k$ is the operating point the rest of our experiments target. It matches TabPFN-v2.5’s native context cap and is the largest context that fits every TFM under parity, even though it represents only about 0.7% of the per-watershed KB. At this size every reasonable coreset spans the flood-response surface, the five methods converge into a narrow band, and FL-Depth still leads. Coreset-XGB in panel (b) follows the same broad ordering but with a much smaller method spread. FL-Depth has a small early lead, but the methods converge quickly as N grows because the tree ensemble absorbs row-selection noise into its fit rather than propagating it like an in-context TFM. XGB therefore acts only as a control here, and we adopt FL-Depth as the default hexagon selector for all coreset-based models in the rest of the paper.

5.2. Experiment 1: Within-Watershed

We investigate how close a coreset-based model gets to the watershed-level supervised reference and how fine-tuning shifts that gap. Using the FL-Depth coreset across

six values of N from 500 to 50k, we evaluate three vanilla TFMs, two per-watershed fine-tuned TabPFN variants, and Coreset-XGB. Full-KB-XGB sets the supervised reference, trained on all 350 training events per watershed. We trace how mean R^2 scales with N to see whether any coreset-based model approaches the reference, then break the $N = 50k$ results down by watershed and quantify how much fine-tuning helps each TFM backbone.

5.2.1. Aggregate Scaling with N

The coreset-based models differ in how steeply they improve with N and in which size brings them closest to the Full-KB-XGB reference. Figure 5 reports the within-watershed mean R^2 at each N for the six coreset-based models and the reference. Coreset-XGB rises monotonically with N but plateaus well below the reference, since the tree ensemble has no pretrained prior and learns only from the coreset. TabICL also rises with N but stays below the TabPFN-v2.6 family across the sweep. Its native context window is much larger than 50k, so the parity cap we apply is conservative for TabICL and leaves it short of its optimum in this regime. Vanilla TabPFN-v2.5 climbs through small N , underperforms in the intermediate N range, then recovers at $N = 50k$, a v2.5 backbone weakness that the v2.6 backbone eliminates. TabPFN-FT-v2.5 anchors weights to each target watershed and smooths the v2.5 mid- N dip, but at $N = 50k$ it still trails Vanilla TabPFN-v2.6. Vanilla TabPFN-v2.6

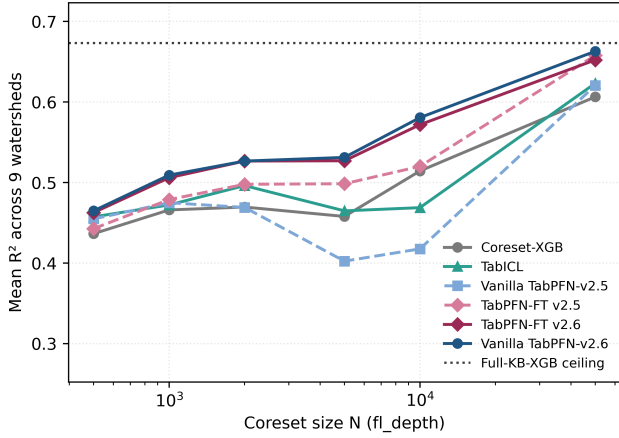


Figure 5: Within-watershed R^2 scaling with coreset size N . Mean R^2 across the nine watersheds for the six coreset-based models under FL-Depth, with the Full-KB-XGB reference shown as the dotted line.

risers monotonically with N and reaches $R^2 = 0.663$ at $N = 50k$, the highest among coreset-based models and a 98.5% recovery of the Full-KB-XGB reference at 0.673. The same fine-tuning recipe applied to v2.6 yields TabPFN-FT-v2.6, which tracks Vanilla TabPFN-v2.6 closely but lands slightly lower. The v2.6 prior already encodes the per-watershed adjustment that fine-tuning extracts from v2.5, and additional fine-tuning over-fits the limited target signal in each watershed’s coreset. Two patterns dominate the sweep. The backbone upgrade from v2.5 to v2.6 delivers a larger gain than fine-tuning v2.5 does, and fine-tuning v2.6 provides no benefit. Vanilla TabPFN-v2.6 is therefore the strongest within-watershed model in this evaluation. The stronger pretrained prior delivers more than per-watershed adaptation on the v2.5 backbone, and on the v2.6 backbone the prior is already too informative for fine-tuning to improve.

5.2.2. Per-Watershed Model Comparison

At $N = 50k$ with the FL-Depth coreset, we evaluate per-watershed performance for each coreset-based model and the Full-KB-XGB reference. Table 4 reports the R^2 values. By training-pool size the nine watersheds fall into three groups. Addicks and Barker are small reservoirs with ≤ 4 events each, Hunting is a small-pool bayou with 18 events, and the other six bayous hold 33 to 84 events. Volatility across watersheds tracks the TFM backbone. Vanilla TabPFN-v2.5 has the widest cross-watershed standard deviation at $\sigma = 0.090$. It reaches above the reference on Hunting and Barker where the supervised model is data-limited by small training pools, but falls well below it on Brays and Greens where larger pools give the reference more signal than v2.5’s 50-event coreset can extract. TabICL is similarly volatile and drops below Coreset-XGB on the harder bayou watersheds, since its column-row attention is designed for much larger contexts than 50k. Per-watershed fine-tuning on the v2.5 backbone reduces σ to 0.073 by anchoring weights to each target watershed, and the v2.6 backbone reduces it to roughly

0.06 regardless of fine-tuning. Backbone strength rather than fine-tuning carries the stability gain. Vanilla TabPFN-v2.6 wins six of the nine watersheds among coreset-based models, with TabPFN-FT-v2.5 taking Barker and Vince-Buffer and Vanilla TabPFN-v2.5 taking Hunting. More striking, Vanilla TabPFN-v2.6 exceeds the Full-KB-XGB reference on Barker, Hunting, and Sims while recovering 93% to 100% on the remaining six. The three reference-beating watersheds share small-to-moderate training pools where the supervised reference itself is data-limited, leaving room for in-context inference with a strong prior to compensate. The remaining six watersheds have larger pools that benefit Full-KB-XGB more than a fixed-size coreset can match. At only 0.7% of the per-watershed training pool, this makes the coreset approach data-efficient at the watershed level.

5.3. Experiment 2: Cross-Watershed LOO

We measure cross-watershed transfer by holding out one target watershed at a time. For each held-out target T , the inference context of size N is built from the other eight watersheds’ 50k-row random coresets, with two source-selection modes determining how those eight pools feed the context. The *geo* mode uses only the K_T watersheds touching T in the mesh-derived adjacency graph of Table 5, each contributing N/K_T rows. The *all* mode uses all eight other watersheds, each contributing $N/8$ rows. The *geo* pool size K_T varies by target, and the mode tests whether watersheds touching T carry sufficiently representative hydrologic regimes that a smaller and more local pool matches the wider pool of all eight. Hexagons within each contributing watershed are sampled at random, since Experiment 1 already characterizes selector effects. We sweep eight context sizes from 1k to 50k and compare three model groups. Vanilla TabPFN on both backbones consumes the cross-watershed context without parameter updates. TabPFN-FTLOO on both backbones is fine-tuned across the other eight watersheds before inference, so that neither the target’s data nor its weights enter the prediction. Coreset-XGB is a tree-based baseline fitted on the same cross-watershed context. The Full-KB-XGB reference from Experiment 1 is not reused here because each of its models was trained on its own watershed’s full training rows and would leak target labels into a leave-one-out evaluation, and keeping every model at the same 50k-row cross-watershed context isolates the transfer effect from data-volume differences. The leave-one-out protocol breaks the spatial leakage that a random k -fold split would not catch (Roberts et al., 2017; Meyer et al., 2018), providing a notion of cross-watershed transfer principled with respect to the spatial structure of the data (Meyer and Pebesma, 2021).

Cross-watershed performance separates cleanly by backbone. Vanilla TabPFN-v2.5 peaks at the smallest N and decays steadily as the context grows, while Vanilla TabPFN-v2.6 holds R^2 between 0.50 and 0.52 across the entire sweep and takes the lead from $N = 10k$ onward. Figure 6 traces the full sweep and Table 6 pins three landmark N values under both modes. The TabPFN-FTLOO variants track

Table 4

Per-watershed R^2 at $N = 50k$ under FL-Depth, with the bottom two rows giving the cross-watershed mean and standard deviation σ . Bold marks each row's coreset-based maximum, and italics mark cells where a coreset-based model exceeds the Full-KB-XGB reference. V-TabPFN denotes Vanilla TabPFN, and TabPFN-FT is the fine-tuned variant.

Watershed	Coreset XGB	TabICL	V-TabPFN v2.5	TabPFN-FT v2.5	TabPFN-FT v2.6	V-TabPFN v2.6	Full-KB XGB
Addicks	0.592	0.605	0.615	0.652	0.651	0.662	0.677
Barker	0.670	0.727	<i>0.766</i>	0.779	0.727	<i>0.749</i>	0.728
Brays	0.557	0.526	0.508	0.586	0.578	0.596	0.617
Cypress	0.631	0.617	0.589	0.642	0.655	0.675	0.697
Greens	0.561	0.553	0.527	0.559	0.580	0.593	0.632
Hunting	0.667	<i>0.757</i>	0.765	<i>0.762</i>	<i>0.745</i>	<i>0.748</i>	0.737
Sims	0.601	0.645	0.607	<i>0.668</i>	<i>0.673</i>	0.680	0.661
Vince-Buffalo	0.589	0.580	0.601	0.630	0.619	0.601	0.649
Whiteoak-Buffalo	0.589	0.600	0.608	0.643	0.642	0.662	0.663
Mean	0.606	0.623	0.621	0.658	0.652	0.663	0.673
Std	0.041	0.076	0.090	0.073	0.058	0.059	0.041

Table 5

Touching-watershed neighbors used by the *geo* mode, derived from mesh-cell geometry.

Target watershed	K_T	Neighbors
Addicks Reservoir	3	Barker, Cypress, Whiteoak-Buffalo
Barker Reservoir	4	Addicks, Brays, Cypress, Whiteoak-Buffalo
Brays Bayou	4	Barker, Sims, Vince-Buffalo, Whiteoak-Buffalo
Cypress Creek	4	Addicks, Barker, Greens, Whiteoak-Buffalo
Greens Bayou	4	Cypress, Hunting, Vince-Buffalo, Whiteoak-Buffalo
Hunting Bayou	3	Greens, Vince-Buffalo, Whiteoak-Buffalo
Sims Bayou	2	Brays, Vince-Buffalo
Vince Bayou-Buffalo Bayou	5	Brays, Greens, Hunting, Sims, Whiteoak-Buffalo
Whiteoak Bayou-Buffalo Bayou	7	Addicks, Barker, Brays, Cypress, Greens, Hunting, Vince-Buffalo

their backbones without overtaking Vanilla TabPFN-v2.6, so leave-one-out fine-tuning offers no usable lift on the stronger backbone, mirroring the within-watershed FT finding from Experiment 1. The mode gap stays narrow across the sweep. The one exception is Coreset-XGB at $N = 50k$ under *all*, where the wider and more diverse training pool benefits tree fitting enough to overtake every TFM. Outside that corner, the narrow mode gap supports the spatial-locality intuition behind *geo*'s design. Touching watersheds carry enough representative variation to substitute for the full eight-watershed pool in cross-watershed transfer. Vanilla TabPFN-v2.6 is

therefore the strongest cross-watershed model, transferring leak-free to a held-out target at the same 50k-row context size as within-watershed inference. As in Experiment 1, per-task fine-tuning is unnecessary on the stronger backbone.

5.4. Experiment 3: Real Events

We evaluate five coreset-based models and the Full-KB-XGB reference on Hurricane Harvey and Tropical Storm Imelda. Each TFM uses its own watershed's coreset as in-context examples. Harvey's storm profile lies entirely

Table 6

Cross-watershed LOO R^2 at $N \in \{2k, 10k, 50k\}$, averaged over nine held-out target watersheds under the *geo* and *all* source-selection modes. Bold marks each row's maximum.

Mode	N	Coreset XGB	V-TabPFN v2.5	TabPFN-FT v2.5	TabPFN-FT v2.6	V-TabPFN v2.6
<i>geo</i>	2k	0.4529	0.5300	0.4641	0.4627	0.5195
	10k	0.4807	0.4790	0.4875	0.5026	0.5152
	50k	0.4795	0.3984	0.4691	0.4954	0.5023
<i>all</i>	2k	0.4660	0.5141	0.4733	0.4690	0.5056
	10k	0.4910	0.5113	0.4533	0.4970	0.5169
	50k	0.4940	0.4097	0.4527	0.4815	0.4851

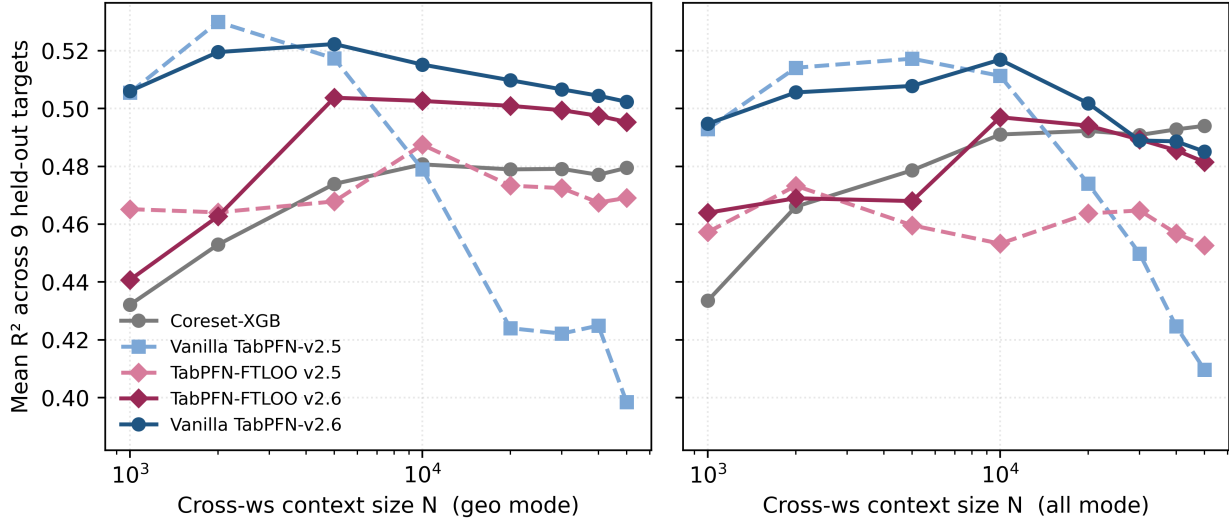


Figure 6: Cross-watershed LOO mean R^2 versus context size N under the *geo* (left) and *all* (right) source-selection modes, averaged over nine held-out target watersheds.

outside the synthetic training envelope on the cumulative-rainfall and duration axes and therefore serves as a fully out-of-distribution test. Imelda has cells both inside and outside this envelope across the nine watersheds.

Table 7

Real-event R^2 on Hurricane Harvey and Tropical Storm Imelda, averaged over the nine watersheds. Two TFM variants exceed the Full-KB-XGB reference on Harvey, while the reference reclaims the lead on Imelda.

Model	Harvey	Imelda
Coreset-XGB	0.471	0.430
TabICL	0.481	0.380
Vanilla TabPFN-v2.5	0.487	0.404
Vanilla TabPFN-v2.6	0.558	0.430
TabPFN-FT-v2.5	0.570	0.457
Full-KB-XGB	0.503	0.528

On Harvey the two top TFM models exceed the Full-KB-XGB reference. The TabPFN pretrained prior generalizes more reliably than tree-based fitting under sharp distribution shift, since XGB must extrapolate beyond its training envelope while the TFM stays inside its own prior. The backbone upgrade from v2.5 to v2.6 delivers $+0.071 R^2$ on Harvey and accounts for most of the 0.012 gap between Vanilla TabPFN-v2.6 and the leading TabPFN-FT-v2.5. On Imelda the Full-KB-XGB reference reclaims the lead. Breaking the event into its in-distribution and OOD slices localizes the gap. Full-KB-XGB pulls ahead on the OOD slice with $+0.13 R^2$ over Vanilla TabPFN-v2.6, while the three top models converge within $0.02 R^2$ on the in-distribution slice. TabPFN-FT-v2.5 retains a $0.027 R^2$ edge over Vanilla TabPFN-v2.6 on this mixed event. This is the only point in the entire evaluation where fine-tuning shows measurable value. In-distribution prediction depends more on training volume

than on the pretrained prior. Full-KB-XGB fits 6.9M rows per watershed and stays ahead of every coreset model on Imelda, while TabPFN-FT-v2.5 extracts more from its 50k coreset through 500 gradient-update episodes than vanilla in-context inference does in a single forward pass. The two storms partition the real-event regime by distribution shift. Coreset TFMs hold more potential than tree-based fitting for far-OOD events, while tree-based models with full training access remain hard to beat on in-distribution events.

6. Conclusion

We present a domain-aware coreset construction pipeline that conditions a tabular foundation model on a small fraction of the training rows used by a watershed-level supervised baseline. With a 50k-row coreset at about 0.7% of the per-watershed training pool, Vanilla TabPFN-v2.6 reaches mean $R^2 = 0.663$ across nine Houston-area watersheds and recovers 98.5% of a Full-KB-XGB reference trained on roughly 6.9M rows per watershed. This makes Vanilla TabPFN-v2.6 the optimal TFM in our evaluation. Three design elements drive this result. Dual stratification of storm events by NOAA Atlas 14 return period and most-affected watershed ensures rare-event coverage. Target-aware spatial selection via FL-Depth picks hexagons that span the flood-response surface. A sufficiently strong pretrained backbone removes the need for per-task fine-tuning. The same model also transfers to a held-out watershed by drawing in-context examples from its touching neighbors, without any gradient updates.

The three experiments map the operating range of the candidates. In the within-watershed evaluation, all coreset TFMs improve with context size N , but the trajectory depends on the backbone. The TabPFN-v2.6 family rises monotonically across the sweep, while the TabPFN-v2.5 family dips through the intermediate N range and recovers

only at $N = 50k$. Vanilla TabPFN-v2.6 reaches the highest mean $R^2 = 0.663$, within 1.5% of the supervised reference on only 0.7% of the per-watershed training data, and per-watershed fine-tuning provides no further benefit. In the cross-watershed leave-one-out evaluation, Vanilla TabPFN-v2.5 peaks at the smallest N and decays as the context grows, while Vanilla TabPFN-v2.6 stays stable between 0.50 and 0.52 across the full sweep and leads the coreset-trained supervised baseline at most context sizes in both source-selection modes. LOO fine-tuning likewise provides no benefit. Two real storms confirm the pattern, with TFMs exceeding the supervised reference on far-ODD Hurricane Harvey and the reference reclaiming the lead on the largely in-distribution Tropical Storm Imelda. Coreset TFMs therefore hold an advantage under far-ODD conditions, while supervised models with full training access remain hard to beat in-distribution.

Several boundaries of the current scope motivate future work. Vanilla TabPFN-v2.6 has higher cross-watershed variance than the Full-KB-XGB reference (std = 0.059 versus 0.041), so its higher mean comes with a wider per-watershed worst case. The 50k-row context cap is well matched to per-watershed inference but leaves room to explore the larger native windows of TabPFN-v2.6 at roughly 100k and TabICL at higher still. The real-event component covers two storms that span the OOD and in-distribution regimes, and the cross-watershed evaluation draws on nine Houston-area watersheds. The mesh-to-H3 conversion standardizes spatial units but gives hexagons inheriting the same mesh cell a shared depth label, so future evaluation should report sensitivity at both the H3 and original mesh-cell resolution. Results here are reported in R^2 , and complementary metrics such as RMSE, MAE, and high-depth tail accuracy would further characterize operational reliability. Future work includes evaluating on a wider set of historical storms, testing transfer across distinct hydroclimatic regions to probe the broader transfer-learning capability of coreset TFMs, and exploring hybrids that combine TFM in-context inference with tree-based fitting on in-distribution residuals.

References

- Bachem, O., Lucic, M., Krause, A., 2017. Practical coreset constructions for machine learning. arXiv preprint arXiv:1703.06476 .
- Bentivoglio, R., Isufi, E., Jonkman, S.N., Taormina, R., 2022. Deep learning methods for flood mapping: A review of existing applications and future research directions. *Hydrology and Earth System Sciences* 26, 4345–4378.
- Chen, T., Guestrin, C., 2016. XGBoost: A scalable tree boosting system, in: *Proceedings of the 22nd ACM SIGKDD International Conference on Knowledge Discovery and Data Mining*, pp. 785–794.
- Coleman, C., Yeh, C., Musmann, S., Mirzasoileiman, B., Bailis, P., Liang, P., Leskovec, J., Zaharia, M., 2020. Selection via proxy: Efficient data selection for deep learning, in: *International Conference on Learning Representations*.
- Conrad, O., Bechtel, B., Bock, M., Dietrich, H., Fischer, E., Gerlitz, L., Wehberg, J., Wichmann, V., Böhner, J., 2015. System for automated geoscientific analyses (SAGA) v. 2.1.4. *Geoscientific Model Development* 8, 1991–2007.
- Esparza, M., Battala, V., Mostafavi, A., 2026. A graph neural network and decision tree modeling approach for predicting wildfire-induced building damage. *Computer-Aided Civil and Infrastructure Engineering* , 100085.
- Grinsztajn, L., Flöge, K., Key, O., Birkel, F., Jund, P., Roof, C., Jäger, L., Hollmann, N., Hutter, F., 2025. TabPFN-2.5: Advancing the state of the art in tabular foundation models. arXiv preprint arXiv:2511.08667 .
- Grinsztajn, L., Oyallon, E., Varoquaux, G., 2022. Why do tree-based models still outperform deep learning on tabular data?, in: *Advances in Neural Information Processing Systems*.
- Harris County Flood Control District, 2023. Harris county flood warning system. <https://www.harriscountyfws.org/>.
- Hollmann, N., Müller, S., Eggensperger, K., Hutter, F., 2023. TabPFN: A transformer that solves small tabular classification problems in a second, in: *International Conference on Learning Representations*.
- Hollmann, N., Müller, S., Purucker, L., Krishnakumar, A., Körfer, M., Hoo, S.B., Schirmmeister, R.T., Hutter, F., 2025. Accurate predictions on small data with a tabular foundation model. *Nature* 637, 319–326.
- Killamsetty, K., Sivasubramanian, D., Ramakrishnan, G., De, A., Iyer, R., 2021a. GRAD-MATCH: Gradient matching based data subset selection for efficient deep model training, in: *International Conference on Machine Learning*, pp. 5464–5474.
- Killamsetty, K., Sivasubramanian, D., Ramakrishnan, G., Iyer, R., 2021b. GLISTER: Generalization based data subset selection for efficient and robust learning, in: *Proceedings of the AAAI Conference on Artificial Intelligence*, pp. 8110–8118.
- Koh, P.W., Sagawa, S., Marklund, H., Xie, S.M., Zhang, M., Balsubramani, A., Hu, W., Yasunaga, M., Phillips, R.L., Gao, I., et al., 2021. WILDS: A benchmark of in-the-wild distribution shifts, in: *International Conference on Machine Learning*, pp. 5637–5664.
- Kratzert, F., Klotz, D., Brenner, C., Schulz, K., Herrnegger, M., 2018. Rainfall-runoff modelling using long short-term memory (lstm) networks. *Hydrology and Earth System Sciences* 22, 6005–6022.
- Lee, C.C., Huang, L., Antolini, F., Garcia, M., Juan, A., Brody, S.D., Mostafavi, A., 2024. Predicting peak inundation depths with a physics informed machine learning model. *Scientific Reports* 14, 14826.
- Li, X., Ma, J., Brody, S.D., Mostafavi, A., 2025. A parametric framework for anticipatory flashflood warning: Integrating landscape vulnerability with precipitation forecasts. arXiv preprint arXiv:2512.17785 .
- Lin, H., Bilmes, J., 2011. A class of submodular functions for document summarization, in: *Proceedings of the 49th Annual Meeting of the Association for Computational Linguistics: Human Language Technologies*, pp. 510–521.
- Ma, J., Li, B., Li, X., Mostafavi, A., 2026. Uncovering spatiotemporal coupling of electricity outages and food access disruptions during disasters. *Transportation Research Part D: Transport and Environment* 156, 105358.
- Meyer, H., Pebesma, E., 2021. Predicting into unknown space? Estimating the area of applicability of spatial prediction models. *Methods in Ecology and Evolution* 12, 1620–1633.
- Meyer, H., Reudenbach, C., Hengl, T., Katurji, M., Nauss, T., 2018. Improving performance of spatio-temporal machine learning models using forward feature selection and target-oriented validation. *Environmental Modelling & Software* 101, 1–9.
- Mirzasoileiman, B., Bilmes, J., Leskovec, J., 2020. Coresets for data-efficient training of machine learning models, in: *International Conference on Machine Learning*, pp. 6950–6960.
- Mosavi, A., Ozturk, P., Chau, K.w., 2018. Flood prediction using machine learning models: Literature review. *Water* 10, 1536.
- Müller, S., Hollmann, N., Pineda Arango, S., Grabocka, J., Hutter, F., 2022. Transformers can do Bayesian inference, in: *International Conference on Learning Representations*.
- National Oceanic and Atmospheric Administration, 2018. NOAA Atlas 14 precipitation-frequency Atlas of the United States. <https://hdsc.nws.noaa.gov/pfds/>. Accessed via the Precipitation Frequency Data Server (PFDS).
- Pak, H., Leach, S., Yoon, S.H., Paal, S.G., 2023. A knowledge transfer enhanced ensemble approach to predict the shear capacity of reinforced concrete deep beams without stirrups. *Computer-Aided Civil and Infrastructure Engineering* 38, 1520–1535.

- Phillips, J.M., 2017. Coresets and sketches. *Handbook of Discrete and Computational Geometry*, 1269–1288.
- Prior Labs, 2025. TabPFN-2.6. https://huggingface.co/Prior-Labs/tabPFN_2.6. Software release supporting up to 100,000 rows and 2,000 features.
- Qu, J., Holzmüller, D., Varoquaux, G., Le Morvan, M., 2024. TabICL: A tabular foundation model for in-context learning on large data. *arXiv preprint arXiv:2502.05564*.
- Roberts, D.R., Bahn, V., Ciuti, S., Boyce, M.S., Elith, J., Guillerá-Arroita, G., Hauenstein, S., Lahoz-Monfort, J.J., Schröder, B., Thuiller, W., Warton, D.I., Wintle, B.A., Hartig, F., Dormann, C.F., 2017. Cross-validation strategies for data with temporal, spatial, hierarchical, or phylogenetic structure. *Ecography* 40, 913–929.
- Rubachev, I., Kotelnikov, A., Kartashev, N., Babenko, A., 2025. On finetuning tabular foundation models. *arXiv preprint arXiv:2506.08982*.
- Sener, O., Savarese, S., 2018. Active learning for convolutional neural networks: A core-set approach, in: *International Conference on Learning Representations*.
- Sorscher, B., Geirhos, R., Shekhar, S., Ganguli, S., Morcos, A., 2022. Beyond neural scaling laws: Beating power law scaling via data pruning. *Advances in Neural Information Processing Systems* 35, 19523–19536.
- Tarboton, D.G., 1997. A new method for the determination of flow directions and upslope areas in grid digital elevation models. *Water Resources Research* 33, 309–319.
- Thomas, V., Ma, J., Hosseinzadeh, R., Golestan, K., Yu, G., Volkovs, M., Caterini, A.L., 2024. Retrieval & fine-tuning for in-context tabular models, in: *Advances in Neural Information Processing Systems*.
- Wahl, T., Jain, S., Bender, J., Meyers, S.D., Luther, M.E., 2015. Increasing risk of compound flooding from storm surge and rainfall for major US cities. *Nature Climate Change* 5, 1093–1097. doi:10.1038/nclimate2736.
- Wei, K., Iyer, R., Bilmes, J., 2015. Submodularity in data subset selection and active learning, in: *International Conference on Machine Learning*, pp. 1954–1963.
- Xiao, Y., Mostafavi, A., 2025. Damagecat: A deep learning transformer framework for typology-based post-disaster building damage categorization. *International Journal of Disaster Risk Reduction*, 105704.
- Xiao, Y., Yin, K., Mostafavi, A., 2026. Crisisense-rag: Crisis sensing multimodal retrieval-augmented generation for rapid disaster impact assessment. *Computer-Aided Civil and Infrastructure Engineering*, 100096.
- Yin, K., Li, B., Mostafavi, A., 2026. Deep learning-driven community resilience rating based on intertwined socio-technical systems features. *npj Urban Sustainability*.
- Yin, K., Mostafavi, A., 2023. Unsupervised graph deep learning reveals emergent flood risk profile of urban areas. *arXiv preprint arXiv:2309.14610*.
- Zahura, F.T., Goodall, J.L., Sadler, J.M., Shen, Y., Morsy, M.M., Behl, M., 2020. Training machine learning surrogate models from a high-fidelity physics-based model: Application for real-time street-scale flood prediction in an urban coastal community. *Water Resources Research* 56, e2019WR027038. doi:10.1029/2019WR027038.
- Zscheischler, J., Westra, S., van den Hurk, B.J.J.M., Seneviratne, S.I., Ward, P.J., Pitman, A., AghaKouchak, A., Bresch, D.N., Leonard, M., Wahl, T., Zhang, X., 2018. Future climate risk from compound events. *Nature Climate Change* 8, 469–477. doi:10.1038/s41558-018-0156-3.